Mathematical and Computational Modeling of Heat Transfer and Deformation in Film Blowing Process

Hossein Ali Khonakdar, J. Morshedian, A. O. Nodehi

Iran Polymer Institute, P.O. Box 14965/115, Tehran, I.R. Iran

Received 8 May 2001; accepted 16 October 2001

ABSTRACT: The blown-film extrusion process was investigated both experimentally and theoretically. In experimental study, nonisothermal experiments were conducted using low-density polyethylene. Rheological parameters were studied, considering the polymer melt as a power law fluid in nonisothermal conditions. Axial tension, bubble diameter, and film thickness at a variety of film extrusion conditions, that is, different flow rate, pressure difference across the film, and take-up speeds were measured. In theoretical study, an analysis was employed to simulate the blown-film extrusion process by setting up the force- and energy-balance equations on the film bubble moving upward. Four nonlinear complex differential equations were integrated numerically, using an iterative backward shooting method and the fifth-order Runge-kutta technique. The program written, based on a mathematical model, predicts the bubble shape, temperature profile, and film thickness as a function of the distance along the machine axis. Furthermore, the model evaluates the elongational viscosity of LDPE in biaxial tension in terms of distance from die axis and take-up speed. In this simulation, the total stress components in machine and the transverse directions were computed from the die exit up to the freeze line, the knowledge of which is necessary for evaluation of the elastic memory build up in heat-shrinkable films. © 2002 Wiley Periodicals, Inc. J Appl Polym Sci 86: 2115–2123, 2002

Key words: extrusion; film blowing; heat transfer; deformation; elongation rate

INTRODUCTION

The production of extruded polyethylene film is a common industrial process that has been the subject of major investigations over many years.[1–4] The blown film process is quite complex but provides considerable flexibility in producing films of various physical and mechanical properties (Fig. 1).[5] It is the overwhelming choice for producing polyethylene film and has been applied to other polymers on a commercial basis as well. This process results in the biaxial orientation of polymer molecules by axial and hoop stretching of the film bubble.[6]

Processing simulation

Figure 2 shows a schematic of the geometry of the film-blowing process. The analysis that follows originates from the work of Pearson and Petrie,[7] who first analyzed the kinematics of tubular film extrusion. The following assumptions are also incorporated in our method to simulate the process: 1) the film thickness is small in comparison with other characteristic dimensions (i.e., $H \ll R$, which is the thin-sheet approximation); 2) die swell is neglected, or the origin of the fixed coordinate system is assumed to be just beyond the maximum of die swell amount, 3) steady-state conditions exist, 4) the fluid bubble is axisymmetric.

The analysis is carried out in terms of a coordinated system, with ξ_1, ξ_2, and ξ_3 embedded in the film, as shown in Figure 2. It is seen that the local velocity gradients e_{11}, e_{22}, and e_{33} are related to the flow rate Q, bubble radius a, film thickness h, and the variation of bubble radius and film thickness along the die axis through the following equations[8]:

$$e_{11} = -\frac{Q \cos\theta}{2\pi a h}\left(\frac{1}{a}\frac{da}{dz} + \frac{1}{h}\frac{dh}{dz}\right); \quad (1)$$

$$e_{22} = \frac{Q \cos\theta}{2\pi a h^2}\frac{dh}{dz}; \quad (2)$$

$$e_{33} = \frac{Q \cos\theta}{2\pi a^2 h}\frac{da}{dz}. \quad (3)$$

Now we are in position to calculate the viscous stresses associated with this deformation. For the Newtonian fluid, we will have[8]

$$T_{ij} = -P\delta_{ij} + \eta_B(\mathrm{II})e_{ij} \quad (i, j = 1, 2, 3), \quad (4)$$

in which P denotes the isotropic pressure, δ_{ij} denotes the kronecker delta, $\eta_B(\mathrm{II})$ is the elongational viscosity

Correspondence to: H. A. Khonakdar (H.khonakdar@proxy.ipi.ac.ir).

Journal of Applied Polymer Science, Vol. 86, 2115–2123 (2002)

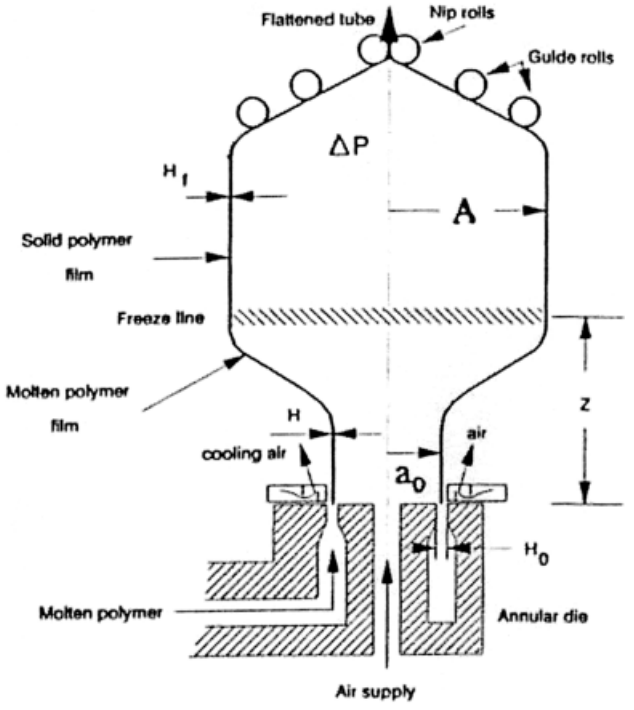

Figure 1 Schematic of the film-blowing process.

in blown film extrusion in general, and II is the second invariant of the rate-of-strain tensor (e), defined as

$$\mathrm{II} = e_{11}^2 + e_{22}^2 + e_{33}^2 + 2(e_{12} + e_{21})^2 + 2(e_{13} + e_{31})^2 + 2(e_{23} + e_{32})^2. \quad (5)$$

It should be noted that, in eqs. (1) to (3), the film is assumed to be planar and thin, and thus the shear components of the rate of strain are negligible.

The stress normal to the free boundary is T_{22}. As a boundary condition, we will assume that no external forces act on the bubble and that surface tension forces are insignificant with respect to viscous forces. Then it follows that

$$T_{22} = 0, \quad (6)$$

and, from eq. (4), we find the isotropic pressure in the fluid to be

$$P = \eta_B(\mathrm{II})e_{22}. \quad (7)$$

Using eq. (7) in eq. (4), we obtain

$$T_{11} = \eta_B(\mathrm{II})(e_{11} - e_{22}) \quad (8)$$

and

$$T_{33} = \eta_B(\mathrm{II})(e_{33} - e_{22}), \quad (9)$$

in which T_{11} is the tensile stress in the direction of flow and T_{33} is the stress in the transverse direction (i.e., the hoop stress).

Therefore, the elongational viscosity in nonuniform biaxial stretching may be represented as

$$\eta_B(\mathrm{II}) = \frac{T_{11}}{e_{11} - e_{22}} \quad (10)$$

or

$$\eta_B(\mathrm{II}) = \frac{T_{33}}{e_{33} - e_{22}}, \quad (11)$$

in which e_{11}, e_{22}, and e_{33} are given by eqs. (1), (2), and (3), respectively.

Force balance equation

The force balance equations are given as[8,9]:

$$2\pi a \cos\theta P_L + \pi\Delta P(A^2 - a^2) + 2\pi\rho g \int_z^Z ah \sec\theta \, dz = F_z, \quad (12)$$

where

$$F_z = F_L - 2\pi\rho_s g AH(L - Z); \quad (13)$$

$$\Delta P = \frac{P_L}{R_L} + \frac{P_H}{R_H} - \rho g h \sin\theta; \quad (14)$$

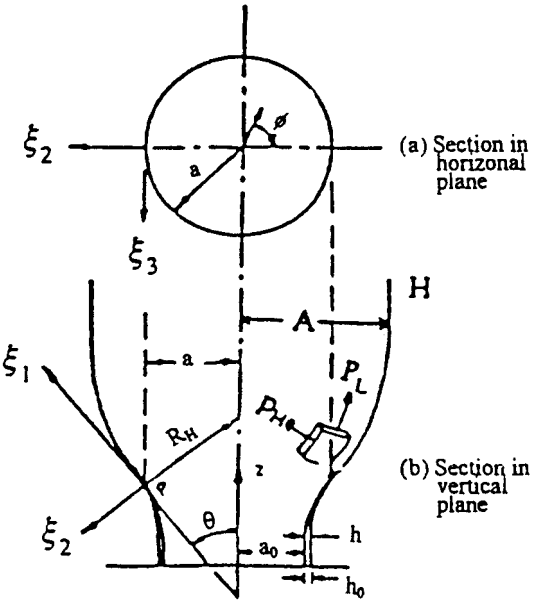

Figure 2 Coordinate systems describing the deformation of a bubble.

$$P_{\mathrm{L}} = \int_0^h T_{11} d\xi_2 = hT_{11}; \tag{15}$$

$$P_{\mathrm{H}} = \int_0^h T_{33} d\xi_2 = hT_{33}; \tag{16}$$

$$R_{\mathrm{H}} = \frac{a}{\cos\theta}; \tag{17}$$

$$R_{\mathrm{L}} = \frac{\sec^3\theta}{\dfrac{d^2a}{dz^2}}, \tag{18}$$

in which a and A are bubble radii at z and Z (the frost line), h is the film thickness at z, P_{L} is the force acting in the direction of film, ΔP is the pressure difference across the film, g is the gravity, P_{H} is the force in the transverse direction, F_Z is the tensile force at $z = Z$, and F_{L} is the tension actually measured at $z = L$.

If one wishes determine the elongational viscosity in the blown film process, one may make use of eq. (8), or eq. (9) for nonuniform biaxial stretching.

For this, one has to take measurements of a, h, and θ as a function of z and the axial tension. Substituting eq. (15), into the left-hand side of eq. (12) and eq. (13) into the right-hand side of eq. (12), we obtain

$$T_{11} = \frac{F_{\mathrm{R}}}{2\pi ah\cos\theta}, \tag{19}$$

where

$$F_{\mathrm{R}} = F_{\mathrm{L}} - \pi\Delta P(A^2 - a^2) - 2\pi\rho g \int_z^Z ah\sec\theta\, d\theta - 2\pi\rho_s g AH(L - Z). \tag{20}$$

Now it can be seen that once measurements of a, h, and θ are taken as a function of z, substituting F_{R} from eq. (20) into eq. (19) permits one to calculate the tensile stress T_{11} and, hence, the elongational viscosity $\eta_B(\mathrm{II})$ for nonuniform biaxial stretching using eq. (10), together with eqs. (1) and (2).

Substituting the values of T_{11}, e_{11} and e_{22} for every element in eq. (8), the elongational viscosity pertaining to that element is obtained. Making use of this parameter along with eqs. (2) and (3) for each element in eq. (9), the total stress components in the hoop direction are computed.

To extend the usefulness of the above force balance equations into the nonisothermal blown film process, we propose the following semiempirical expression for the Generalized Newtonian fluid function[10]:

$$\eta_B(\mathrm{II}, T) = \eta_0\, EXP\left[\frac{E}{R}\left(\frac{1}{T} - \frac{1}{T_0}\right)\right]\left[\frac{\mathrm{II}}{2}\right]^{n-1/2}, \tag{21}$$

where II is the second invariant of rate of strain tensor, T is the film temperature, η_0 is the zero shear rate viscosity at reference temperature T_0, E is the activation energy, R is the gas constant, and n is a material constant.[11,12]

Using dimensionless variables, $r = a/a_0$, $w = h/a_0$, $x = a/a_0$, and $s = T/T_0$, and with aid of geometrical relationships and eqs. (14)–(18), (8), (1), and (2), eqs. (12) and (13) may be rewritten as follows[11,12]:

$$\frac{w'}{w} = -\frac{r'}{2r} - \frac{\eta_0[T_g + r^2B]\sec^2\theta}{4\eta_B(\mathrm{II}, s)}; \tag{22}$$

$$2r^2[T_g + r^2B]r'' = \frac{6r'\eta_B(\mathrm{II}, s)}{\eta_0} + r\sec^2\theta\,[T_g - 3r^2B], \tag{23}$$

where

$$B = \frac{a_0^3\pi\Delta P}{Q\eta_0}; \tag{24}$$

$$T_g = \frac{a_0}{Q\eta_0}\left[F_z - 2\pi\rho g a_0^3\int_x^X rw\sec\theta\, dx\right] - B\left[\frac{A}{a_0}\right]^2; \tag{25}$$

$$X = \frac{Z}{a_0}. \tag{26}$$

Using the geometrical relationship (Fig. 2), we have

$$\frac{da}{dz} = \tan\theta, \tag{27}$$

which may be rewritten in terms of the dimensionless variable:

$$r' = \tan\theta; \tag{28}$$

$$r'' = \sec^2\theta\theta'. \tag{29}$$

Substituting eqs. (28) and (29) into eq. (23), we obtain

$$2r^2[T_g + r^2B]\theta' = \frac{3\sin 2\theta\eta_B(\mathrm{II}, s)}{\eta_0} + r[T_g - 3r^2B]. \tag{30}$$

The term $\eta_B(\mathrm{II}, T)$ may be expressed in terms of dimensionless variables as

TABLE I
Some Important Numerical Values of the Physical Parameters Used in This Simulation

Material	Reference temp. (°C)	α	β	E cal/mol	n	ρ g/cc	ρ_s g/cc	η_0
Low-density polyethylene	200	3592	3.504	2948.13	0.375	0.718	.918	28572.9

$$\eta_B(\mathrm{II}, s) = \alpha \exp\beta/s\left[\frac{Q\cos\theta}{2\pi a_0^3}\right]^{n-1}\left[\frac{1}{rw}\right]^{n-1} \times\left[\left(\frac{w'}{w}\right)^2+\left(\frac{r'}{r}\right)^2+\left(\frac{r'w'}{rw}\right)\right]^{n-1/2}, \quad (31)$$

where

$$\alpha = \eta_0 e^{-E/RT}, \quad \beta = \frac{E}{RT_0}.$$

In the above equations w', r', and θ' are the first-order derivatives of w, r, and θ with respect to x.

Energy balance equation

Based on the assumptions stated above, an energy balance on the film may be written as follows[11,13]:

$$\rho C_v v_1 \frac{\partial T}{\partial \xi_1} = \frac{\partial q}{\partial \xi_2}, \quad (32)$$

in which ρ is the fluid density, C_v is the specific heat capacity, v_1 is the velocity in ξ_1 direction, and q is the heat flux in ξ_2 direction. Multiplying both sides of eq. (21) by $d\xi_2$ and integrating from $\xi_2 = 0$ to $\xi_2 = h$ results:

$$\rho C_v \frac{Q\cos\theta}{2\pi a}\frac{dT}{dz} = U(T - T_a) + \lambda\varepsilon(T^4 - T_a^4), \quad (33)$$

in which the following boundary conditions were used:

(1) at $\xi_2 = 0$ (inner surface),

$$q = 0; \quad (34)$$

(2) at $\xi_2 = \mathrm{h}$ (outer surface),

$$q = U(T - T_a) + \lambda\varepsilon(T^4 - T_a^4), \quad (35)$$

where U is the overall heat transfer coefficient, λ is the Stefan–Boltzmann constant, ε is emissivity, T_a is the ambient temperature, and Q is the volumetric flow rate. Using dimensionless variables, eq. (33) may be rewritten as follows[8,14];

$$q = rD\sec\theta(s - s_a) + rE(s^4 - s_a^4), \quad (36)$$

where

$$D = (UT_0)/\left(\frac{\rho C_v Q T_0}{2\pi a_0^2}\right), \quad E = (T_0^4\lambda\varepsilon)/\left(\frac{\rho C_v Q T_0}{2\pi a_0^2}\right),$$

in which s is the dimensionless temperature, s' is the derivative of s with respect to x, and D and E are dimensionless parameters.

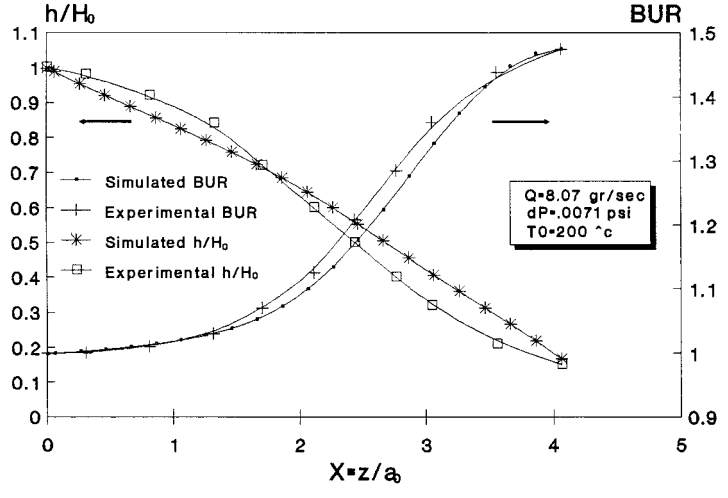

Figure 3 Calculated variation of blow-up-ratio and film thickness versus axial distance from die head with incomparison experimental results.

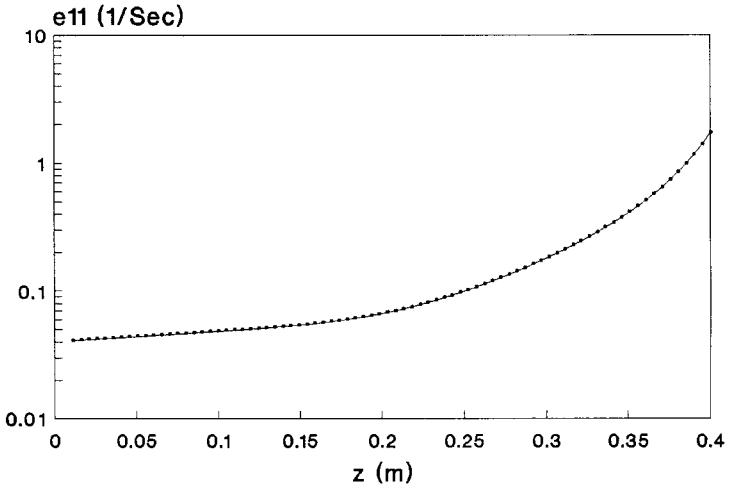

Figure 4 The local velocity gradient versus axial distance from die head.

Governing system equation and computational procedure

For simulating the nonisothermal blown film process by a non-Newtonian fluid of power law type, one has to solve eqs. (22), (28), (30), and (36) with the aid of eqs. (25) and (31). Concerning the intense relation of the variables to one another, solution of the collective differential–integral equations is very complex.

In this work, the above equations, using an irritation method in inverse manner, were integrated by fifth-order Runge-Kutta technique from condition (I) to condition (II):

$$\text{I)}\ x = X = \frac{Z}{a_0},\ r = \frac{A}{a_0},\ w = \frac{H}{a_0},\ s = \frac{T_s}{T},\ \theta = 0,$$

$$\text{II)}\ x = 0,\ r = 1,\ w = \frac{h_0}{a_0},\ s = 1,\ \theta = \theta_0.$$

At first, the effect of gravity on T_g parameter was ignored in the calculation; however, later, the equations were solved by considering the above effect on modification of T_g.

Then we checked whether eq. (25) was satisfied. If eq. (25) was not satisfied, numerical integration of eqs. (22), (28), (30), and (36) was repeated with new guesses of T_g until it was satisfied. This computational procedure was found to be very effective in the actual simulation study.

EXPERIMENTAL

Experimental studies were carried out on LDPE blown film in nonisothermal condition. In this respect, operational parameters such as pressure difference, temperature, stretching force, and so forth were measured in film-blowing processing conditions.

Pressure difference was evaluated using a water manometer linked to the die air entry valve.

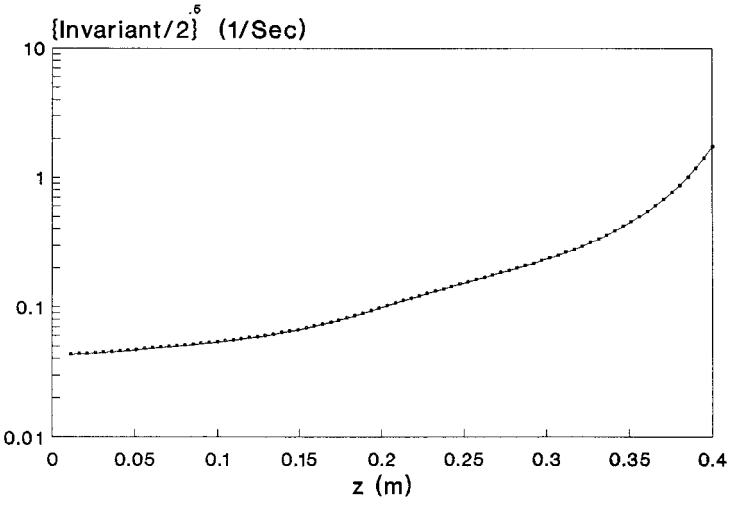

Figure 5 The elongation rate versus axial distance from die head.

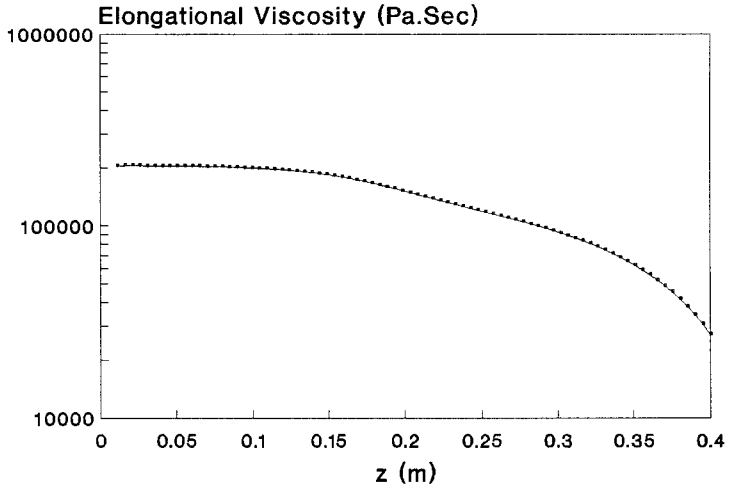

Figure 6 The elongational viscosity versus axial distance from die head.

In view of practically measuring the bubble radius and thickness variations, the extruder and take-off were simultaneously set off with the upward moving bubble stopped instantly as a result. The bubble was cooled down by means of air circulation around its circumference and later was blade cut from the die exit point. This allowed one to measure bubble radius and thickness variation up to the freeze line above where the radius remains constant.

The material constants (n and η_0) needed in our simulation were calculated from viscosity measurements in different temperatures and shear rates. The capillary rheometer used was model 3211 made by Instron (Bucks, UK). The film density, ρ_s, was determined using the alcohol–water column technique. The densitometer used was of gradient type made by Daventest Ltd. (Welwyn Garden, UK).

In Table I, some numerical values of the physical parameters of interest in our simulation are shown. Standard engineering correlation for U as stated below has been wrongly used in some discussions of the process[12]:

$$U = K_1(W_{\max})^n;$$

where $n = 1.5$, $K_1 = 4\ \mathrm{wm}^{-2}\ k^{-1}$ being the best guess from limited data, and $W_{\max}$ is the maximum velocity of cooling air at any distance from the die.

RESULTS AND DISCUSSION

We observed that the bubble shape was extremely sensitive to the variation in air pressure within the bubble. As may be expected, bubbles of different shapes give rise to films of different thicknesses. For a fixed flow rate, the take-up speed was found to be a very sensitive variable affecting the film thickness. Of course, a meaningful variable would be the stretch ratio (V_L, V_0), which is defined as the ratio of the linear

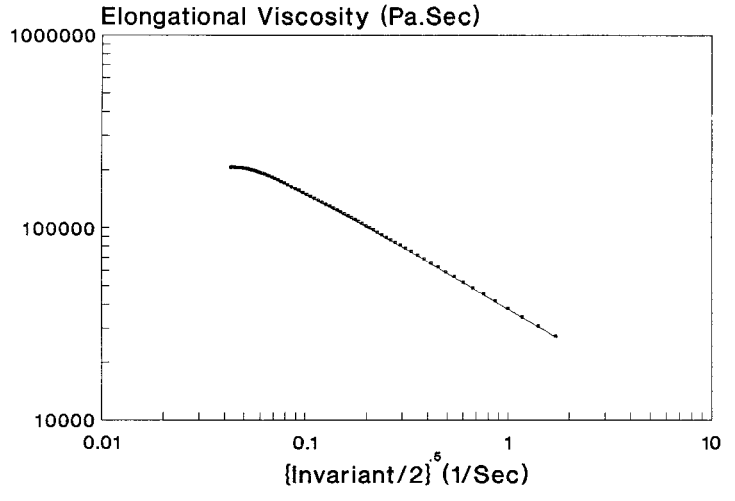

Figure 7 The elongational viscosity versus elongation rate in biaxial stretching.

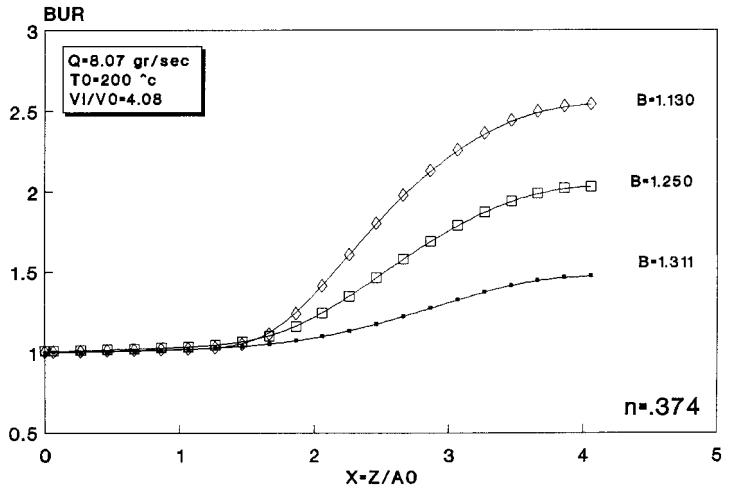

Figure 8 Effect of pressure difference 'B' on the shape of the film bubble (BUR) in the machine direction (z).

velocity at the take-up device to the average linear velocity of the melt at the die exit.

Having measured the bubble radius a, film thickness h, and the angle θ as functions of machine direction z, we were able to calculate the elongation rate and blow-up ratio at different values of z. Figure 3 shows calculated variations of blow-up ratio and film thickness versus axial distance from die head in comparison with experimental results. A good agreement between the two is distinguishable.

Figure 4 shows the local velocity gradient versus axial distance for biaxial stretching. It can be seen in Figure 4 that the local velocity gradient increases with axial distance (i.e., machine direction z).

Figure 5 shows the elongation rate versus axial distance. The elongation rate increases with axial distance.

Figures 6 and 7, respectively, show the elongational viscosity versus axial distance from die head and elongation rate in biaxial stretching.

It is clear that elongational viscosity decreases with increasing of axial distance from die head and increasing elongation rate.

Figure 8 shows the effect of pressure difference as reflected by the parameter, B, in machine direction on the bubble blowing up. Contrary to what was expected, the blow-up ratio is seen to decrease profoundly with increasing B.

This may be explained using the Laplace law ($\Delta P = \sigma/a$) for the balance of surface tension with the air pressure inside the bubble, which results in bubble shrinkage with pressure uprise. Figure 9 shows the effect of pressure (as seen by the parameter B) on the film temperature profile in machine direction. It is clear that with increasing B, the bubble shrinks and, as a result, the final film temperature is enhanced.

Figure 10 shows the total stress component versus axial distance from die head. With increasing of axial distance from die head, tensile stress in the direction

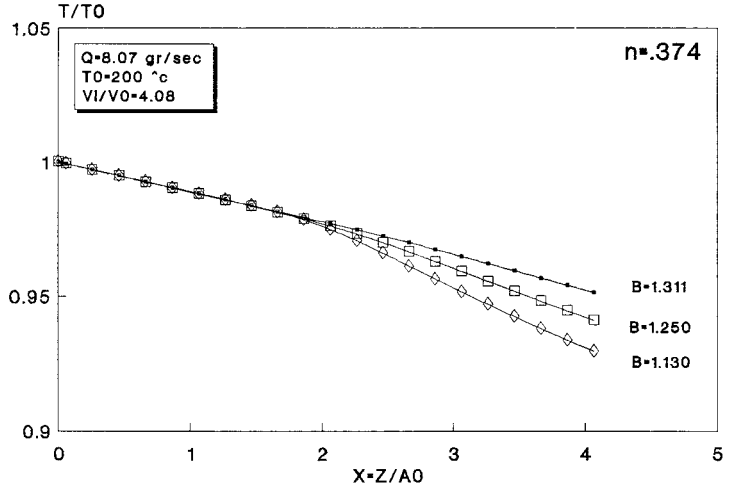

Figure 9 Effect of pressure difference 'B' on the temperature profile (T/T_0) of the film bubble in the machine direction (z).

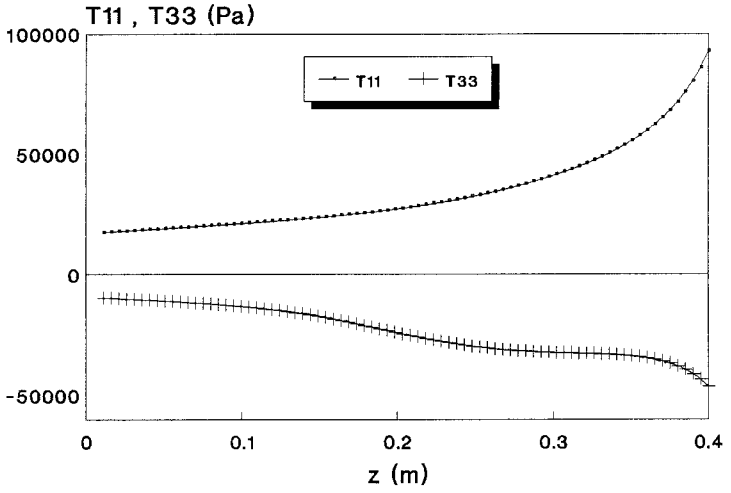

Figure 10 The total stress component versus axial distance from die head.

of flow (T_{11}) in increased and tensile stress in the transverse direction (T_{33}) is decreased.

CONCLUSION

The blown film-processing simulation made on the basis of the proposed mathematical model can reasonably predict the amount of bubble blowing, film thickness profile, and temperature profile in terms of operational variables such as pressure difference (ΔP) and stretch ratio (V_L/V_0).

Also, a power law type of empirical expression for describing the rheological property pertinent to the blown film process has been used, relating the elongational viscosity to the second invariant of the rate-of-strain tensor in biaxial stretching.

The very good agreement observed is a credit to the validity of the established model. The efficiency of the model becomes more profound when considering the effect of gravity on the film elevation, enabling it to be advantageous in industrial scale.

Because, in trace of the shear velocity matrix, e_{11} is the velocity gradient in the direction of film movement, it increases with distance from the die. With increase in distance from the die, one expects the viscosity to be increased owing to the polymer melt cooling down; however, because of the pseudoplastic nature of the melt in flow, it is decreased instead. Furthermore, with increasing distance from the die, as the bubble cools rapidly, the stress can hardly relax and, thus, remains in the frozen film. This effect is responsible for the building up of some elastic memory in the film, some amount of which determines the percentage of the heat shrinkability of film. Moreover, as it is seen in Figure 10, as the change in stress components in the film direction is considerably higher than that in the hoop direction, the heat shrinkability is more pronounced in the longitudinal axis.

NOMENCLATURE

A	bubble radii at Z
a	bubble radii at z
a	bubble radii at $z = 0$
P	isotropic pressure
δ_{ij}	kronecker delta
$\eta_B(II)$	elongational viscosity
II	second invariant of the rate-of-strain tensor (e)
e_{11}	local velocity gradients
e_{22}	local velocity gradients
e_{33}	local velocity gradients
T_{11}	tensile stress in the direction of flow
T_{33}	tensile stress in the transverse direction (i.e., the hoop stress).
h	film thickness at z
H	film thickness at Z
P_L	force acting in the direction of film
P_H	force in the transverse direction
ΔP	pressure difference across the film
g	gravity
F_Z	tensile force at $z = Z$
F_L	tension actually measured at $z = L$
T	film temperature
η_0	zero shear rate viscosity at reference temperature T_0
E	activation energy
R	gas constant
n	material constant
T_0	reference temperature
ξ_1, ξ_2, and ξ_3	coordinated system
ρ	fluid density
C_v	specific heat capacity
v_1	velocity component in ξ_1 direction
v_2	velocity component in ξ_2 direction
v_3	velocity component in ξ_3 direction
q	heat flux in ξ_2 direction
U	overall heat transfer coefficient
λ	Stefan–Boltzmann constant
ε	emissivity
T_a	ambient temperature
Q	volumetric flow rate
s	dimensionless temperature
s'	derivative of s with respect to x

D and E	dimensionless parameters
η_0	material constants
ρ_s	density of solid film
(V_L/V_0)	stretch ratio
T_{ij}	total stress component
R_L, R_H	principal radii of curvature of the film

References

1. White, J. L.; Spruiell, J. E. Polym Eng Sci 1983, 23, 247.
2. Gilbert, M.; Hemsley, D. A.; Patel, S. A. Brit Poly J 1987, 19, 9.
3. Pazur, R. J.; Prudhomme, R. E. Macromolecules 1996, 29, 119.
4. Yu, T.-H.; Wilkes, G. L. Polymer 1996, 37, 4675.
5. Baird, D. G.; Collias, D. I. Polymer Processing; Wiley, 1998.
6. Chandran, P.; Jabarin, S. Adv Polym Tech 1993, 12, 119.
7. Pearson, J. R. A.; Petrie, C. J. S. Mechanical Principles of Polymer Processing; Pergamon, 1966.
8. Han, C. D.; Park, J. Y. J Appl Polym Sci 1975, 29, 3257.
9. Pearson, J. R. A.; Petrie, C. J. S. Plast Polym 1970, 38, 85.
10. Bird, R. B.; Armstorng, R. C.; Hassager, O. Dynamics of Polymer Liquids, Vol. 1: Fluid Mechanics; 2nd ed. Wiley: New York, 1987.
11. Middleman, S. Fundamentals of Polymer Processing; Mcgraw-Hill, 1977.
12. Pearson, J. R. A.; Richardson, S. M. Computational Analysis of Polymer Processing; Applied Science Publishers: London, 1983.
13. White, J. L.; Cakmak, M. Adv Polym Tech 1988, 8, 27.
14. Kanai, T.; White, J. L. Polym Eng Sci 1984, 24, 1185.